

Oxide-supported IrNiO_x core-shell particles as efficient, cost-effective, and stable catalysts for electrochemical water splitting**

Hong Nhan Nong, Hyung-Suk Oh, Tobias Reier, Elena Willinger, Marc-Georg Willinger, Valeri Petkov, Detre Teschner*, Peter Strasser*

Abstract: Active and highly stable oxide-supported IrNiO_x core-shell catalysts for the electrochemical water splitting are presented. IrNi_x@IrO_x nanoparticles supported on high surface-area mesoporous antimony-doped tin oxide (IrNiO_x/Meso-ATO) were synthesized from bimetallic IrNi_x precursor alloys (PA-IrNi_x/Meso-ATO) using electrochemical Ni leaching and concomitant Ir oxidation. Special emphasis was placed on Ni surface segregation under thermal treatment of the PA-IrNi_x/Meso-ATO, as well as the surface chemical state of the particle/oxide support interface. Combining a wide array of characterizations we uncovered the effect of segregated NiO phases on the water splitting activity of core-shell particles. The core shell IrNiO_x/Meso-ATO catalyst displayed high water splitting activity and unprecedented stability in acidic electrolyte providing substantial progress in the development of PEM electrolyzer anode catalysts with drastically reduced Ir loading and significantly enhanced durability.

Water electrolysis, combined with renewable electric power generation technologies, such as solar electric, solar-thermal, hydro, or wind power plants, is expected to emerge as a low-emission method for storing excess electricity and for producing hydrogen fuel as part of a solar refinery.¹⁻⁶ The challenge in electrocatalytic water splitting is the high overpotential required for the anodic oxygen evolution reaction (OER),^{7,8} which hinders the development and application of devices to convert sunlight or electricity into storable fuels. Acid Polymer Electrolyte Membrane (PEM) electrolyzers show critical advantages compared to alkaline electrolyzers in terms of system design, load flexibility, current densities, voltage efficiency, and gas purity.⁹ However, there are two major challenges associated with a larger-scale implementation of PEM electrolyzers. First, the acidic environment of PEM electrolyzers requires the use of scarce and expensive noble metals, such as Ru or Ir.¹⁰⁻¹³ Given

the chemical instability of RuO_x catalysts, IrO_x appears as the catalyst of choice.^{3,14-19} However, the scarce nature of Ir requires significant reduction of Ir loading, which is why core-shell nanoarchitectures are highly beneficial to achieve this goal. For example, carbon supported IrNi core-shell nanoparticles^{20,21} were found to be highly active for the hydrogen reduction reaction, IrNi metallic core IrO_x shell nanoparticles²² showed enhanced activity for OER at low Ir content. Nevertheless, the core-shell catalysts must be supported on corrosion-stable and highly conductive support materials to ensure sufficient durability of PEM electrolyzers. Note that carbon materials undergo oxidative degradation during OER and thus are not suitable here.

In the present contribution, we address the challenges related to noble metal content and durability of water splitting catalysts presenting a low-Ir content OER catalyst with previously unachieved electrochemical performance durability. To accomplish this goal, we utilized a conductive, corrosion-resistant oxide material with exceptionally high surface area to support Ir-Ni oxide nanoparticles (NPs) with a IrNi@IrO_x core-shell architectures.²² The core-shell structure helped to tune the intrinsic electrocatalytic activity, while lowering the Ir content significantly. The IrNiO_x core-shell structure was obtained from IrNi nanoparticle precursor alloys using electrochemical selective dealloying of Ni and a simultaneous surface oxidation of the surface Ir atoms resulting in the IrO_x shells. Emphasis was placed on an atomic-scale understanding of surface and bulk chemical transformations and segregations during the preparation and during the catalytic operation of the core shell catalysts. To the best of our knowledge, this is the first report of a low-Ir content core-shell oxide catalyst combined with a corrosion-stable oxide support resulting in a highly active and remarkably stable water splitting electrocatalyst.

A number of different IrNi_x (x=3.3 to 3.8) NP precursor alloys supported on mesoporous antimony doped tin oxide (IrNi_x/Meso-ATO) were prepared starting with the synthesis of Meso-ATO powder supports using a soft-templating process involving tetradecylamine (TDA) as template.²³ Thereafter, IrNi_x metallic NPs were synthesized using a polyol method in the presence of 1,2-tetradecandiol as reducing agent and oleic acid, oleylamine as capping agents.²² Meso-ATO powder was introduced into reaction mixture before starting the metal reduction. The supported NPs were washed with ethanol, freeze dried and then thermally treated at different temperatures T (T = 180, 250, 300, 400, 500 °C). The obtained precursor alloys were denoted as PA-IrNi_x/Meso-ATO-T, and later used for synthesis of the core-shell structured catalysts (IrNiO_x/Meso-ATO-T). For comparison, pure Ir NPs supported on commercial ATO (Ir/com.-ATO) and carbon (Ir/C) were also synthesized. The detailed synthetic protocols of the support and catalysts are presented in the Supporting Information (SI).

The TEM image of the Meso-ATO powder (Fig. 1a) shows a mesoporous, foam-like structure consisting of interconnected NPs with exceptional monodispersity. This structure provides a surface area as high as 264 m² g⁻¹²³ and thus is much higher

[*] Prof. Dr. P. Strasser, Dr. H.S. Oh, H.N. Nong, T. Reier
Department of Chemistry, Technical University Berlin
Strasse des 17. Juni 124, TC 03, 10623 Berlin, Germany
E-mail: pstrasser@tu-berlin.de

Prof. Dr. V. Petkov
Department of Physics, Central Michigan University
Mt. Pleasant, MI 48859, USA
Dr. D. Teschner, Dr. E. Willinger, Dr. M.G. Willinger
Department of Inorganic Chemistry, Fritz-Haber-Institut der Max-Planck-Gesellschaft
Faradayweg 4-6, D-14195 Berlin, Germany
E-Mail: teschner@fhi-berlin.mpg.de

[**] We thank Zelmi of the Technical University. Financial support by the German Research Foundation (DFG) through grant STR 596/3-1 under the Priority Program 1613 is gratefully acknowledged. The work was funded in part by DOE grant DE-SC0006877. H.N. Nong acknowledges financial support by The Socialist Republic of Vietnam and the German Academic Exchange Service (DAAD). We thank HZB for allocation of synchrotron radiation beamtime. Many helpful discussions with Robert Schloegl are gratefully acknowledged.

Supporting information for this article is given via a link at the end of the document.

than that of commercial ATO (Sigma Aldrich, $\sim 47 \text{ m}^2 \text{ g}^{-1}$). IrNi_x alloy NPs showed a fairly homogeneous dispersion with a few small agglomerated clusters (Figure 1b and inset). The nanoparticle size distributed in the range of $7.3 \pm 2.5 \text{ nm}$.

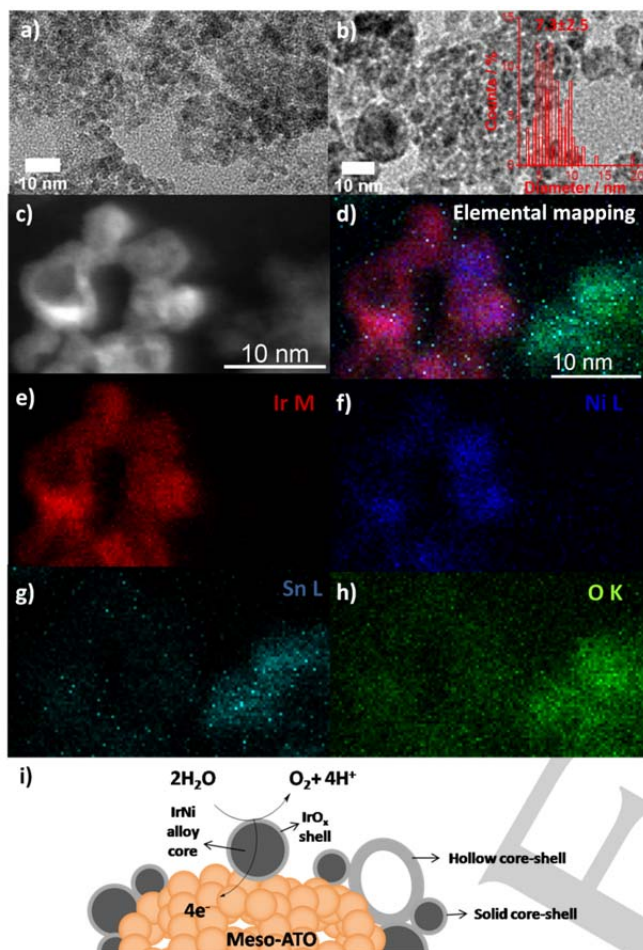


Figure 1. a) TEM image of mesoporous ATO (Meso-ATO), b) TEM image of Meso-ATO supported IrNi_{3.3} nanoparticle (NP) precursor alloy annealed at 180 °C (PA-IrNi_{3.3}/Meso-ATO-180), inset is size distribution of IrNi_{3.3} NPs, c) HAADF-STEM image of the IrNiO_x/Meso-ATO-180 core-shell NP catalysts synthesized from PA-IrNi_{3.3}/Meso-ATO-180, d) Elemental mapping of Fig. 1c, e), f), g), h) Elemental mappings of Ir, Ni, Sn, and O in Fig. 1c, respectively, i) scheme of the oxygen evolution reaction on the IrO_x shell of IrNiO_x core-shell NPs supported on Meso-ATO.

The preparation of metallic alloy NPs supported on redox active oxides and the removal of capping agents require a careful optimization of a balanced annealing protocol in order to maintain the chemical state of alloy and support. In this study, the materials were annealed in inert N₂ gas, as opposed to our previous procedure in H₂,²² to prevent the reduction of ATO support. Thermal treating of a bimetallic nano alloy in different atmosphere could lead to different atomic segregation phenomena, affecting the catalytic reactivity of the alloy.²⁴ Therefore, we first investigated the effects of thermal treatment on the atomic structure of the PA-IrNi_x/Meso-ATO-T and on the OER activity of the obtained core-shell catalysts. The structure

of the PA-IrNi_x/Meso-ATO-T were studied by powder X-ray diffraction patterns (XRD), X-ray photoelectron spectroscopy (XPS) and high energy XRD coupled with atomic pair distribution function (HE-XRD PDFs), the results are presented in Fig. 2.

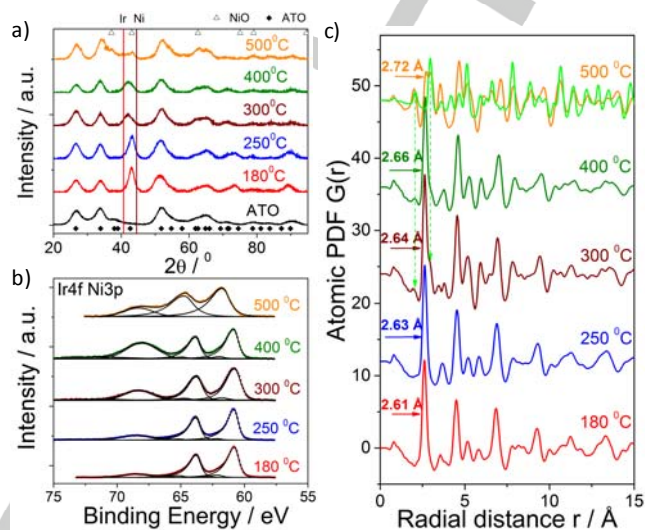


Figure 2. Characterization of supported IrNi_x precursor alloys annealed at different temperatures T (T is given by each data set). a) XRD patterns, vertical solid lines indicate (111) database reflections of pure metallic Ir and Ni; open triangles and solid rhombuses indicate database main reflections of NiO and antimony-doped tin oxide, respectively, b) Ir4f Ni3p XPS spectra measured at kinetic energy of 550 eV, and c) Experimental atomic pair distribution functions (PDFs). Radius of first atomic coordination sphere in NPs is given by each data set. Signatures of NiO nanophase appear with samples treated at 300 °C and above (green vertical broken arrows), and the NiO nanophase fully developed in the sample annealed at 500 °C (solid green line).

XRD patterns of PA-IrNi_x/Meso-ATO-T with T ≤ 400 °C (Fig. 2a) showed typical reflections between 40 and 45°, corresponding to (111) planes of the alloy crystallites.²² The reflections dropped in intensity and shifted to smaller 2θ with increasing T, indicating enrichment in Ir at decreased crystallite size. The XRD pattern of the sample treated at 500 °C (Fig. 2a, orange line) shows additional reflections corresponding to NiO, indicating the transformation of metallic Ni to oxide.

Core level photoemission spectra in the Ir4f Ni3p range of the PA-IrNi_x/Meso-ATO-T materials (Fig 2b) confirmed metallic Ir at the surface for T < 500 °C. The Ni2p spectra of all PA-IrNi_x/Meso-ATO-T (Fig.S1) evidenced the presence of Ni(II) oxide²² while only the low-T samples maintained metallic surface Ni (~852.6 eV). Thus, we conclude that only the low-T samples maintained the desired Ir-Ni metallic alloy phase suited for dealloying and core-shell formation. Compositional surface and bulk analysis of the IrNi_x/Meso-ATO-T samples (Table S1) revealed an increasing Ni excess in the particle surface, peaking at 400 °C. This points to Ni segregation of amorphous and, at higher T, crystalline Ni oxide phases and is quite similar to Ni segregation reported in PtNi nanoparticles.²⁴ At 500 °C, both Ni and Ir display an oxidized chemical state.

Atomic PDF patterns extracted from the HE-XRD data are shown in Fig. 2c. The patterns are corrected for support scattering and thus directly reflect the 3D atomic structure of the IrNi_x NPs. The first atomic coordination shell (2.61 Å) of the PA- $\text{IrNi}_{3.3}/\text{Meso-ATO-180}$ is consistent with a substitutional solid solution (random) alloy of Ir and Ni atoms falling in-between the metal-metal distances of pure Ni (~2.49 Å) and pure Ir (~2.71 Å). The increasing first shell radial distance with annealing temperature confirmed Ir bulk segregation, in agreement with powder XRD and XPS results. Signatures of a cubic NiO nanophase appeared at 300 °C (vertical green broken lines in Fig. 2c) developing into a prominent co-existing NiO nanophase at $T = 500$ °C (green solid line). Remnants of metallic NPs have first coordination sphere positioned at 2.72 Å which is very close to the atomic size of pure Ir.

Experimental and model atomic PDFs for the various $\text{IrNi}_x/\text{Meso-ATO-T}$ samples are presented in Fig. S2. Models feature fcc-type (red line) metallic alloy and NiO nanophase (blue line). NPs treated at 180 °C and 250 °C are metallic nanoalloys of fcc-type structure, though the fcc structure is somewhat “distorted”. NPs treated at 500 °C are completely phase segregated into a metallic Ir and NiO phase. Missing signatures of bulk IrO_2 suggested that IrO_x observed in XPS existed only near-surface. Based on our understanding of the thermal behavior of the $\text{IrNi}_x/\text{Meso-ATO-T}$ precursors, we hypothesized that annealing at 180 °C ($\text{IrNi}_{3.3}/\text{Meso-ATO-180}$ material) would be most amenable to the generation of the core-shell oxide architecture.

We utilized oxidation by voltammetric cycling²² to generate alloy core - oxide shell nanoparticles from the $\text{IrNi}_x/\text{Meso-ATO-T}$ precursor alloys. Electrochemically oxidized Ir NPs (Ir/C and Ir/com.-ATO) were used as activity and stability reference. The oxidized $\text{IrNi}@\text{IrO}_x$ core-shell catalysts and benchmarks were denoted as “ $\text{IrNiO}_x/\text{Meso-ATO-T}$ ”, “ IrO_x/C ”, and “ $\text{IrO}_x/\text{com.-ATO}$ ”, respectively.

Figure 1c displays an aberration-corrected HAADF-STEM Z-contrast image of the $\text{IrNiO}_x/\text{Meso-ATO-180}$ catalyst. The dealloyed NPs exhibit dark centers with bright outer shells. Under Z-contrast condition, the image intensity of Ir ($Z = 77$) is much higher than that of Ni ($Z = 28$). The spherical morphologies of the NPs rule out thickness variations as source of the dark particle Z-contrast suggesting a dramatically Ir-depleted chemical state of the particle cores surrounded by IrO_x shells. Elemental mapping (Fig 1d, e, f, g, h) confirmed the structural core-shell hypothesis. Analysis of an ensemble of core shell particles revealed that the core-shell morphology depended on particle size, which was also observed for IrNi_x/C .²² Ni was leached from the core of large particles resulting in hollow core-shell structure, whereas smaller particles formed core-shell particles with Ni rich cores. The size distribution of the larger hollow particles is in the range of 7 to 11 nm, for the small Ni rich particles, the diameter is below 4.5 nm (see Fig.S3 and the SI). In order to explain the formation of hollow particles during electrochemical dealloying, we recall that the surface diffusion rate of the more noble metal must be slower than the surface dissolution rate of the less noble metal to allow continuous dealloying deep into the bulk and lead to nanoporosity.²⁵ The nanoporosity formation therefore depends on particle size,²⁶ composition of the alloy,²⁷ dealloying conditions such as

electrolyte and the applied potential.^{27, 28} In the current study, the IrNi_x precursor alloys were dealloyed and oxidized by cycling the potential from 0.05V to 1.5V vs. RHE in N_2 saturated 0.05M H_2SO_4 , at which the dissolution rate of Ni was very high, therefore, the critical particle size to form hollow core-shell structure was small. Another possible explanation for the structure evolution is the atomic structure of the IrNi_x precursor alloys. Since Ni precursor was heated to reaction temperature first and Ir precursor was added afterwards, a number of seeds of Ni might have already formed, and these would result in the bigger particles with Ni-rich cores. HRTEM suggested that the bigger particles are relatively irregular with many defects and multiplet structures. Once a part of Ni has already precipitated, compositionally more uniform smaller IrNi_x nanoparticles were formed. These two types of nanoparticles dealloy differently, resulting in different final morphologies.

To understand the changes in the surface chemical state of Ir during the formation of the active $\text{IrNiO}_x/\text{Meso-ATO-180}$ core-shell catalyst, depth-resolved XPS was applied and the data are shown in Figure 3. Upon cycling into OER electrode potentials, the largely metallic precursor alloy (Fig. 3a) gradually depleted in Ni and transformed into a thin IrO_x shell (Fig. 3b). The oxide shell is however much thinner as compared to IrNiO_x on carbon. Nevertheless, extended OER operation is going to thicken the oxidized surface shell. The 210 eV kinetic energy data evidenced a higher binding energy species, the assignment of which is however not unambiguous. It might be related to final state shift due to size or strain effects but it can also signal the formation of a higher-valent ($> 4+$) Ir state at the top surface layer, as reported recently.⁸

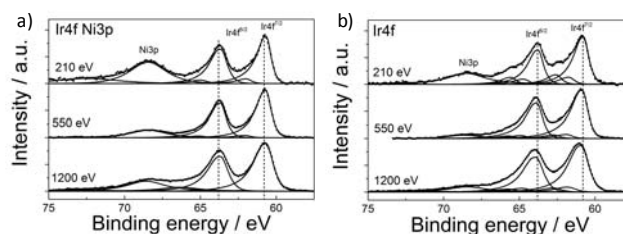


Figure 3. Depth-resolved Ir4f (and Ni3p) XPS spectra of a) PA- $\text{IrNi}_{3.3}/\text{Meso-ATO-180}$ and b) the corresponding $\text{IrNiO}_x/\text{Meso-ATO-180}$ OER catalyst after dealloying and oxidation (50 CV cycles, 0.05-1.5V). Top to bottom spectra were measured at photoelectron kinetic energies of 210, 550, and 1200 eV. The dash vertical lines indicate peak position of metallic Ir. Note, the broader spectra at higher photon energy are due to the lower resolution of the beamline.

Fig. 1i illustrates conceptually our structure hypothesis regarding the active catalyst/support couple, with the OER proceeding at thin IrO_x shells on Ir-low/Ir-free cores, thereby reducing the required Ir amount significantly.

In order to correlate the catalyst structure with its catalytic OER activity under approximate conditions of PEM electrolyzers, the catalysts were subjected to a sweep voltammetry protocol in highly acidic electrolyte.²² The linear sweep voltammetry of all catalysts along with their Ir-mass based reactivity at an overpotential $\eta = 280$ mV are presented in Fig. 4a, b.

Clearly, the $\text{IrNiO}_x/\text{Meso-ATO-T}$ catalysts with $T \leq 300^\circ\text{C}$ are significantly more OER active on both geometric surface and Ir-mass basis compared to the IrO_x/C and $\text{IrO}_x/\text{com.-ATO}$ benchmarks. For these materials, the Ni content in the particle core remained high. It is plausible that, as a result of this, electronic and/or strain effects modified the chemisorption and reactivity of intermediates at the surface. In contrast, the catalysts annealed at 400°C and 500°C , showed significantly lower OER activities due to the phase segregation into a NiO and an Ir-rich nanophase. The lower Ni content of the latter phase translates in a reactivity approaching that of pure Ir. In addition, a smaller $\text{Ir}^{\text{III/IV}}$ wave in the voltammetry of the two high-T catalysts (Fig. S4a) indicated a smaller number of accessible $\text{Ir}^{\text{III/IV}}$ active sites.²² Together, these effects reduce the apparent OER activity of $\text{IrNiO}_x/\text{Meso-ATO}$ annealed at 400°C and 500°C . The most active catalyst was the $\text{IrNiO}_x/\text{Meso-ATO-180}$ material, showing a 2.5 times higher Ir-mass based activity compared to IrO_x/C and $\text{IrO}_x/\text{com.-ATO}$ at $\eta=280\text{ mV}$. This implies a 2.5x times higher electrolyzer hydrogen output at constant voltage.

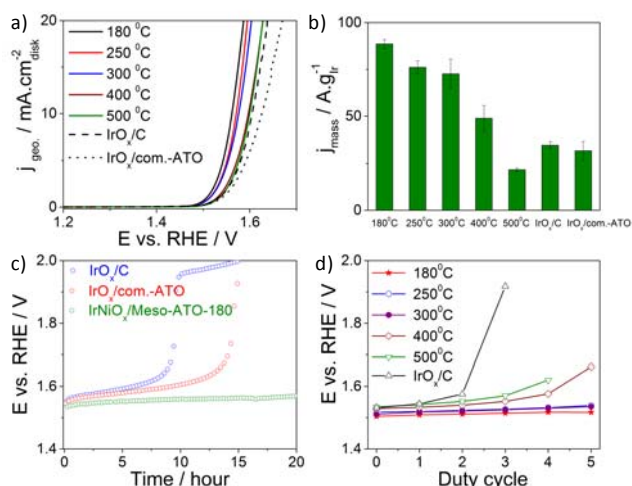


Figure 4. a) Electrocatalytic oxygen evolution reaction (OER) activities of IrNiO_x core-shell nanoparticles (NPs) supported on mesoporous ATO ($\text{IrNiO}_x/\text{Meso-ATO-T}$), pure Ir supported on carbon (IrO_x/C), and on commercial ATO ($\text{IrO}_x/\text{com.-ATO}$) measured using linear sweep voltammetry, b) Ir-mass based activity at $\eta=280\text{ mV}$ overpotential of IrO_x/C , $\text{IrO}_x/\text{com.-ATO}$, and $\text{IrNiO}_x/\text{Meso-ATO-T}$, c) Constant current chronopotentiometric stability measurements at a current density of 1 mA cm^{-2} , and d) Potential at 1 mA cm^{-2} using linear sweep voltammetry after duty cycles of IrO_x/C and $\text{IrNiO}_x/\text{Meso-ATO-T}$. Temperature at which NPs have been treated is given for each data set. Measurement conditions: 25°C , $0.05\text{ M H}_2\text{SO}_4$, 1600 rpm . The loading of Ir was $10.2\text{ }\mu\text{g cm}^{-2}$.

The electrochemical stability of the core-shell $\text{IrNiO}_x/\text{Meso-ATO-180}$ catalyst was tested together with the reference materials under constant current load conditions (chronopotentiometry) for a period of 20 hours (Fig. 4c). The measured electrode potential increased gradually for the IrO_x/C and $\text{IrO}_x/\text{com.-ATO}$, indicating their performance degradation. Then, the electrode potential rose sharply to 2.0 V after 9 and 12 hours for IrO_x/C and $\text{IrO}_x/\text{com.-ATO}$, respectively, evidencing a

severe degradation of the support associated with a loss of the active catalyst particles. In contrast, the electrode potential of $\text{IrNiO}_x/\text{Meso-ATO-180}$ remained essentially constant throughout the 20 hour stability test, evidencing a previously unachieved performance durability of low Ir content core-shell particles.

In order to test the durability of the catalysts under conditions closer to the operating conditions of PEM electrolyzers, we applied a more severe potential-step duty-cycle protocol (Fig. S4b), in which the potential was first kept at $E^{0.5}$ (where current density reached 0.5 mA cm^{-2}) for a period of 10 minutes, then increased by 20 mV and kept at the new value for 10 minutes. This increasing step was repeated for 5 times until the last holding potential E^{final} equaled to $E^{0.5} + 100\text{ mV}$. The process from the holding potential of $E^{0.5}$ to E^{final} was then called one duty cycle. The duty cycle was repeated for 5 times, and after each duty cycle the OER activity was tested by the cyclic voltammetry technique. Fig. 4d plots the electrode potentials at a current density of 1 mA cm^{-2} measured using linear sweep voltammetry after each duty cycle was applied. The electrode potential of IrO_x/C reached $> 1.9\text{ V}$ after only 2 duty cycles, indicating the complete degradation of the catalyst. Note that the same catalyst IrO_x/C was completely degraded after 9 hours in the chronopotentiometry test, showing that testing condition in the stair-case duty cycle protocol was harsher. The $\text{IrNiO}_x/\text{Meso-ATO-500}$ and $\text{IrNiO}_x/\text{Meso-ATO-400}$ were degraded after 4 and 5 duty cycles, respectively. Interestingly, the $\text{IrNiO}_x/\text{Meso-ATO-500}$ was more stable than IrO_x/C although it was less active in the first OER test, benefiting from high corrosive stable Meso-ATO. As before, $\text{IrNiO}_x/\text{Meso-ATO}$ annealed at lower T showed higher activity as well as durability than Ir core-shell catalysts annealed at high T (400 and 500°C). Again, the most active and stable catalyst was the $\text{IrNiO}_x/\text{Meso-ATO-180}$ material evidencing a successful combination of the activity advantages of core-shell architectures and the durability benefits of an oxide support.

In conclusion, we have presented a novel catalyst/support couple concept, involving an electrochemically dealloyed IrNi core- IrO_x shell concept combined with a mesoporous corrosion-resistant oxide support for highly efficient and stable OER catalysts in acidic medium. This concept builds upon the formation of a thermodynamically frustrated oxidized Ir shell that provided excellent OER activity at low noble metal content and the high surface area mesoporous structure of the support enabled the dispersion of the active NPs, as well as provided high corrosive resistance for the catalysts. Correlating the synthesis-structure characteristic with OER activity we concluded that the *IrNiO_x/Meso-ATO-180 core-shell water splitting catalyst supported a 2.5 times higher oxygen, and correspondingly higher hydrogen evolution rate on the electrolyzer level, while showing negligible degradation during a 20 hour stability test unlike various Ir benchmark materials.* The nanostructured core shell catalyst/mesoporous support couples could serve as suitable coatings in realistic PEM electrolyzer anodes. Beyond their practical deployment, the presented core-shell catalyst/oxide support concept represents a quite general strategy to reduce the amount of scarce elements in catalytic nanoparticles, and could be transferred to other precious metal based oxides in the future.

Keywords: IrNi core-shell electrocatalysts, oxygen evolution reaction, X-ray photoelectron spectroscopy, atomic pair distribution function, oxide support, corrosion resistance

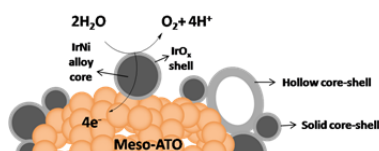
- [1] *Chemical Energy Storage* Schloegl, R., Ed.; De Gruyter Berlin, 2013.
- [2] Forgie, R.; Bugosh, G.; Neyerlin, K. C.; Liu, Z. C.; Strasser, P. *Electrochem. Solid State Lett.* **2010**, *13*, D36.
- [3] Reier, T.; Oezaslan, M.; Strasser, P. *ACS Catalysis* **2012**, *2*, 1765.
- [4] Bergmann, A.; Zaharieva, I.; Dau, H.; Strasser, P. *Energy Environ. Sci.* **2013**, *6*, 2745.
- [5] Neyerlin, K. C.; Bugosh, G.; Forgie, R.; Liu, Z.; Strasser, P. *J. Electrochem. Soc.* **2009**, *156*, B363.
- [6] Dau, H.; Limberg, C.; Reier, T.; Risch, M.; Roggan, S.; Strasser, P. *ChemCatChem* **2010**, *2*, 724.
- [7] Pfrommer, J.; Lublow, M.; Azarpira, A.; Göbel, C.; Lücke, M.; Steigert, A.; Pogrzeba, M.; Menezes, P. W.; Fischer, A.; Schedel-Niedrig, T.; Driess, M. *Angewandte Chemie* **2014**, *126*, 5283.
- [8] Sanchez Casalongue, H. G.; Ng, M. L.; Kaya, S.; Friebel, D.; Ogasawara, H.; Nilsson, A. *Angewandte Chemie International Edition* **2014**, *53*, 7169.
- [9] Carmo, M.; Fritz, D. L.; Mergel, J.; Stolten, D. *Int. J. Hydrog. Energy* **2013**, *38*, 4901.
- [10] Ma, L.; Sui, S.; Zhai, Y. *Int. J. Hydrog. Energy* **2009**, *34*, 678.
- [11] Millet, P.; Mbemba, N.; Grigoriev, S. A.; Fateev, V. N.; Aukauloo, A.; Etiévant, C. *Int. J. Hydrog. Energy* **2011**, *36*, 4134.
- [12] Song, S.; Zhang, H.; Ma, X.; Shao, Z.; Baker, R. T.; Yi, B. *Int. J. Hydrog. Energy* **2008**, *33*, 4955.
- [13] Reier, T.; Teschner, D.; Lunkenbein, T.; Bergmann, A.; Selve, S.; Kraehnert, R.; Schlögl, R.; Strasser, P. *J. Electrochem. Soc.* **2014**, *161*, F876.
- [14] Gorlin, Y.; Jaramillo, T. F. *Journal of the American Chemical Society* **2010**, *132*, 13612.
- [15] Sardar, K.; Ball, S. C.; Sharman, J. D. B.; Thompsett, D.; Fisher, J. M.; Smith, R. A. P.; Biswas, P. K.; Lees, M. R.; Kashtiban, R. J.; Sloan, J.; Walton, R. I. *Chem. Mat.* **2012**, *24*, 4192.
- [16] Kokoh, K. B.; Mayousse, E.; Napporn, T. W.; Servat, K.; Guillet, N.; Soyez, E.; Grosjean, A.; Rakotondrainibé, A.; Paul-Joseph, J. *Int. J. Hydrog. Energy* **2014**, *39*, 1924.
- [17] Ouattara, L.; Fierro, S.; Frey, O.; Koudelka, M.; Comninellis, C. *Journal of Applied Electrochemistry* **2009**, *39*, 1361.
- [18] Antolini, E. *ACS Catalysis* **2014**, *4*, 1426.
- [19] Badia-Bou, L.; Mas-Marza, E.; Rodenas, P.; Barea, E. M.; Fabregat-Santiago, F.; Gimenez, S.; Peris, E.; Bisquert, J. *The Journal of Physical Chemistry C* **2013**, *117*, 3826.
- [20] Sasaki, K.; Kuttiyiel, K. A.; Barrio, L.; Su, D.; Frenkel, A. I.; Marinkovic, N.; Mahajan, D.; Adzic, R. R. *The Journal of Physical Chemistry C* **2011**, *115*, 9894.
- [21] Zhang, W.; Li, L.; Ding, W.; Chen, S.; Wang, H.; Wei, Z. *Journal of Materials Chemistry A* **2014**, *2*, 10098.
- [22] Nong, H. N.; Gan, L.; Willinger, E.; Teschner, D.; Strasser, P. *Chemical Science* **2014**, *5*, 2955.
- [23] Oh, H.-S.; Nong, H. N.; Strasser, P. *Advanced Functional Materials, Accepted* **2014**.
- [24] Ahmadi, M.; Behafarid, F.; Cui, C.; Strasser, P.; Cuenya, B. R. *ACS Nano* **2013**, *7*, 9195.
- [25] Gan, L.; Heggen, M.; O'Malley, R.; Theobald, B.; Strasser, P. *Nano Lett.* **2013**, *13*, 1131.
- [26] Snyder, J.; McCue, I.; Livi, K.; Erlebacher, J. *Journal of the American Chemical Society* **2012**, *134*, 8633.
- [27] Erlebacher, J.; Aziz, M. J.; Karma, A.; Dimitrov, N.; Sieradzki, K. *Nature* **2001**, *410*, 450.
- [28] Erlebacher, J. *J. Electrochem. Soc.* **2004**, *151*, C614.

Entry for the Table of Contents (Please choose one layout)

Layout 1:

COMMUNICATION

IrNiO_x core-shell nanoparticles consisting of a thin IrO_x shell and a Ir-low/Ir-free core supported on mesoporous antimony doped tin oxide is demonstrated to provide substantial advances toward more efficient, stable and less expensive electrolytic water splitting catalysts.



Hong Nhan Nong, Hyung-Suk Oh,
Tobias Reier, Elena Willinger, Marc-
Georg Willinger, Valeri Petkov, Detre
Teschner*, Peter Strasser*

Page No. – Page No.
Oxide-supported IrNiO_x core-shell
particles as efficient, cost-effective, and
stable catalysts for electrochemical
water splitting